

Review of QCD, QGP, Heavy Quark Meson Production Enhancement and Suppression

Leonard S. Kisslinger¹

Department of Physics, Carnegie Mellon University, Pittsburgh, PA 15213

1) kissling@andrew.cmu.edu

Abstract

This review of the Quantum Chromodynamics (QCD), the early universe Cosmological Phase Transition from the Quark-Gluon Plasma (QGP) to our present universe (QCDPT), Relativistic Heavy Ion Collisions (RHIC) which can produce the QGP, the possible detection of the QGP produced by the production of mixed hybrid heavy quark mesons. We also review recent studies of the production of mixed heavy quark hybrids via RHIC and heavy quark meson suppression in p-Pb and Pb-Pb collisions.

Keywords: Quantum Chromodynamics, QCD Phase Transition, Quark-Gluon Plasma, mixed hybrid heavy quark mesons

PACS Indices:12.38.Aw,13.60.Le,14.40.Lb,14.40.Nd

1 Introduction

This Review of Quantum Chromodynamics (QCD), Quark-Gluon Plasma (QGP), and Relativistic Heavy Ion Collisions (RHIC) is based in part on our recent review[1].

We first briefly discuss quarks and gluons, the elementary particles of QCD and components of the QGP. Next Cosmological Phase Transitions and the QCD Phase Transition (QCDPT), with the quark condensate the latent heat, are reviewed. Then the magnetic wall created by bubble collisions during the first-order QCDPT, and how this could lead to correlations in the Cosmic Microwave Background Radiation, is discussed. The contrast between predictions of CMBR Correlations using standard QCD and predictions using string theory or inflationary models is presented.

The theory of mixed normal and hybrid heavy quark states for charmonium and bottomonium mesons and the recent research showing that these mixed hybrid states are produced with enhanced cross sections compared to normal meson states in RHIC is reviewed.

The possibility that experimental measurements of the production of mixed heavy quark hybrid states via RHIC could prove the production of the early universe QGP via heavy atomic nuclear collisions with sufficient energy to reach the temperature of the universe at a time about one millionth of a second after the Big Bang is briefly discussed.

Finally, recent publications on the suppression of these mixed hybrid state in p-Pb and Pb-Pb collisions are reviewed.

2 A Review of Quantum Chromodynamics (QCD)

Quantum Chromodynamics (QCD) is the theory of strong interactions. The basic elementary particles are quarks, fermions with quantum spin 1/2, and gluons, boson with quantum spin 1.

The quark quantum field is q_f , with f the flavor. The quark flavors are $q_f : u, d, s, c, b, t$ =up, down, strange, charm, bottom, and top quarks. The most important quarks flavors for the present review are the charm and bottom quarks. The quarks have three colors. The heavy quark masses, which are important for this review, are $m_c \simeq 1.5$ GeV and $m_b \simeq 5.0$ GeV.

A_μ^a is the strong interaction field, called the gluon field, with the quanta called gluons, and a is the color with gluons having 8 colors. The interaction of quarks with gluons is

$$\begin{aligned} V_{qg} &= \sum_f \bar{q}_f \gamma^\mu g_s A_\mu q_f \\ A_\mu &= \sum_1^8 A_\mu^a \lambda^a / 2, \end{aligned} \quad (1)$$

where the quanta of A_μ are gluons, γ^μ are the Dirac matrices and g_s is the strong interaction coupling constant.

The λ^a are the SU(3) color matrices, with

$$\lambda^a \lambda^b - \lambda^b \lambda^a = i 2 \sum_{c=1}^8 f^{abc} \lambda_c, \quad (2)$$

with f^{abc} the SU(3) structure constants. See [2] for a discussion of color, λ^a , f^{abc} , and quark-gluon interactions.

Note that the strong interaction field, A_μ^a , is similar to the familiar electromagnetic (EM) field, A_μ^{EM} , with the quantum of A_μ^{EM} being the photon. The strength of coupling of charged particles to photons is the electric charge e for the electromagnetic field, as g is the strength of coupling of quarks to gluons. The EM interaction of particles with electric charge e with photons is

$$V_{ep} = i \bar{\psi} \gamma^\mu e A_\mu^{EM} \psi, \quad (3)$$

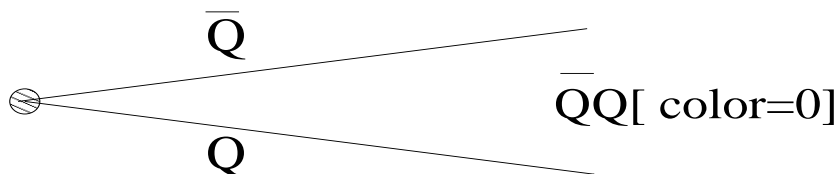
where ψ is a quantum field with electric charge e .

Since $g_s \gg e$, Feynman diagrams can be used for the EM interaction but not for the strong interaction. Nonperturbative methods such as QCD sum rules used to derive the mixed heavy quark hybrids, discussed below, must be used.

2.1 Standard and hybrid heavy quark mesons

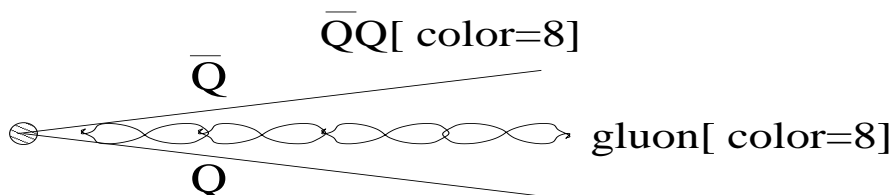
In this review a main element is that the production of mixed heavy quark hybrid mesons can be used for the detection of the QGP via RHIC.

In this subsection we briefly discuss standard heavy quark and hybrid heavy quark mesons. A standard meson consists of a quark and an antiquark with color = 0, while a hybrid meson consists of a quark and an antiquark with color = 8 bound with a gluon with color = 8, with the hybrid meson having color = 0. This is illustrated in the figures below, with the Heavy quark $Q = c$ (charmonium) or $Q = b$ (bottomonium).



Standard Heavy Quark Meson

Figure 1: A meson (color=0) formed by heavy quark bound with an anti-quark



Heavy Quark Hybrid

Figure 2: A hybrid meson (color=0) formed by heavy quark anti-quark of color 8 bound with a gluon of color 8

3 Classical and Quantum Phase Transitions

A classical first order phase transition is the transformation of a system with a well-defined critical temperature, T_c from one phase of matter to another. A quantum phase transition is the transformation from a quantum state to a different quantum state. The QCD Phase Transition (QCDPT) is a Cosmological phase transition in which the state of the universe transforms to a different state of the universe.

3.1 Classical Phase Transitions and Latent Heat

During a first order phase transition as one adds heat the temperature stays at $T = T_c$ until all the matter has changed to the new phase. The heat energy that is added is called latent heat.

A familiar example of a first order phase transitions is ice, a solid, melting to form water, a liquid; and water boiling to form steam, a gas. Note that in addition to solid-liquid and liquid-gas, there are gas-plasma phase transitions, as is the QCDPT, discussed below.

3.2 A Brief Review of Quantum Theory Needed for Cosmological Phase Transitions

In quantum theory one does not deal with physical matter, but with states and operators. A quantum phase transition is the transition from one state to a different state. For the study of Cosmological Phase Transitions a state is the state of the universe at a particular time and temperature.

A quantum state represents the system, and a quantum operator operates on a state. For instance, a system is in state $[1]$ and there is an operator A .

$$\begin{aligned} |[1] > &\equiv \text{state}[1] \\ A &\equiv \text{operator } A . \end{aligned} \quad (4)$$

An operator operating on a quantum state produces another quantum state. For example, operator A operates on state $[1]$

$$A|[1] > = |[2] > , \quad (5)$$

where state $[2]=|[2] >$ is a quantum state. If a system is in a quantum state, the value of an operator is given by the expectation value. For example, consider state $[1] >$ and operator A .

$$\begin{aligned} <[1]| &\equiv \text{adjoint of state}[1] \\ <[1]|A|[1] > &\equiv \text{expectation value of } A . \end{aligned} \quad (6)$$

3.3 Cosmological Phase Transitions

Calling $|0, T >$ the state of the universe at time t when it has temperature T , an operator A has the expectation value $<0, T|A|0, T >$, as discussed above. If there is a cosmological first order phase transition, then there is a critical temperature T_c and

$$<0, T|A|0, T >_{T < T_c} - <0, T|A|0, T >_{T > T_c} = \Delta A , \quad (7)$$

with ΔA the latent heat of the cosmological phase transitions.

It has been shown via lattice gauge theory that the QCDPT is a first order cosmological phase transformation that occurred $t \simeq 10^{-5}$ seconds after the Big Bang, with the critical temperature $kT_c^{QCDPT} \simeq 150 \text{ MeV}$, where k is the Boltzman constant. For $t < 10^{-5} \text{ s}$ the universe is a QGP, while $t > 10^{-5} \text{ s}$ the universe is our present universe.

During the QCDPT bubbles of our present universe with protons, neutrons, etc (hadrons) nucleated within the universe with a dense plasma of quarks and gluons, the Quark-Gluon Plasma (QGP), that existed when the temperature of the universe was greater than T_c^{QCDPT} .

We shall discuss the possible detection of the QGP via relativistic heavy ion collisions (RHIC), but first we discuss the latent heat for the QCDPT and then the mixed hybrid heavy quark states which might detect the QGP produced via RHIC.

3.4 The QCDPT and Quark Condensate

As reviewed above, the QCD fermion fields and particles are quarks. The Latent Heat for the QCD Phase Transition (QCDPT) is the Quark Condensate. With the notation $q(x)$ = the quark field and $\bar{q}(x)$ = the antiquark field,

$$\begin{aligned} |0, T\rangle &= \text{vacuum state temperature} = T \\ \langle 0, T | \bar{q}(x)q(x) | 0, T \rangle &= \text{quark condensate} \\ \langle 0, T | \bar{q}(x)q(x) | 0, T \rangle &= 0 \text{ in quark gluon plasma phase } T > T_c^{QCDPT} \\ &\simeq -(.23 \text{ GeV})^3 \text{ in hadron phase } T < T_c^{QCDPT} \end{aligned}$$

The quark condensate $\langle \bar{q}q \rangle$ goes from 0 to $(.23)^3 \text{ GeV}^3$ at the critical temperature T_c^{QCDPT} of about 150 MeV, and is therefore a first order phase transition, with the latent heat = $(.23)^3 \text{ GeV}^3$.

Although we do not discuss Dark Energy in this review, note that Dark Energy is cosmological vacuum energy, as is the quark condensate. It has been shown that Dark Energy at the present time might have been created during the QCDPT via the quark condensate[3].

4 Magnetic Wall From QCDPT and CMBR

As a first order phase transition, during the QCDPT bubbles of our hadronic universe form, collide, and form a magnetic wall. This wall produces B-type Cosmic Microwave Background Radiation (CMBR) polarization correlations.

4.1 Magnetic wall produced during the QCDPT

The bubbles of the hadronic (nucleon) phase that form during the QCDPT, as shown in Fig.4, are composed mainly of glue. When two of the bubbles collide they form an interior wall, similar to colliding soap bubbles, made of gluons. The nucleons within the hadronic bubble interact with the interior gluonic wall, and because of symmetry violation are oriented perpendicular to the wall. This creates a magnetic wall, shown in Figure 3

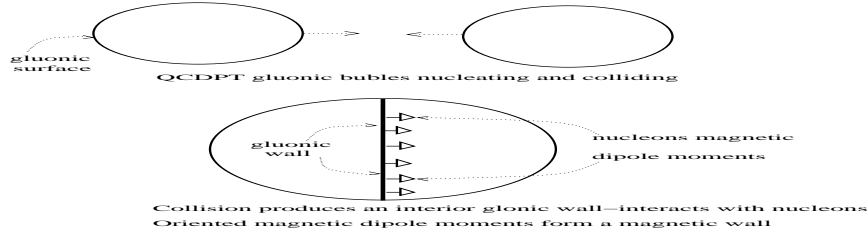


Figure 3: Magnetic wall created during the QCDPT

The magnitude of the magnetic field (B-field) produced during the QCDPT was estimated in [4] in an article motivated in part by improved CMBR observations, which promised polarization correlation measurements, and that these magnetic structures could be primordial seeds of galactic and extra-galactic magnetic fields, a long-standing problem of astrophysics.

Using the mathematical form of [5], including estimates of the lifetime of the interior QCD gluonic wall, the magnetic wall was formed by the interaction of the nucleons with the gluonic wall. The electromagnetic interaction (see Eq(3)) is

$$V_{int}^{EM} = ie\bar{\Psi}\gamma^\mu A_\mu^{EM}\Psi, \quad (8)$$

where Ψ is the nucleon field operator and A_μ^{EM} the EM field discussed above.

This leads to the electromagnetic interaction with the nucleons magnetic dipole moment given in terms of the electromagnetic field tensor, $F^{\mu\nu}$ by

$$\mathcal{V}^{int} = \frac{e}{2M_n}\bar{\Psi}\sigma_{\mu\nu}\gamma_5\Psi F^{\mu\nu}, \quad (9)$$

and a similar interaction (without the γ_5) for the electric dipole moment, due to cp violation. From Eq.(9) one can estimate the magnetic field in the wall. For the gluonic instanton wall oriented in the x-y direction one obtains for $B_z \equiv B_W = F^{21}$ within the wall of thickness ρ

$$B_z \simeq \frac{1}{\rho\Lambda_{QCD}}\frac{e}{2M_n} \langle \bar{\Psi}\sigma_{21}\gamma_5\Psi \rangle. \quad (10)$$

The matrix element in Eq.(10) is estimated using the Fermi momentum in the plane of the wall during the QCD phase transition as Λ_{QCD} , giving $\langle \bar{\Psi}\sigma_{21}\gamma_5\Psi \rangle = \frac{4\pi}{(2\pi)^2}\Lambda_{QCD}^2$. The resulting magnitude of the magnetic field at the wall is (see [6] for derivation of factor 3/14).

$$B_W \simeq \frac{3e}{14\pi}\Lambda_{QCD}. \quad (11)$$

Therefore this picture is that at the end of the QCD phase transition there is a magnetic wall in the hadronic phase in momentum space, derived from the Fourier Transform of $B_W(x)$ [4],

$$\mathbf{B}_W(\mathbf{k}) = \frac{B_W}{2\sqrt{2}b^2M_n}e^{-(k_x^2+k_y^2)/4b^2}e^{-k_z^2/4M_n^2}, \quad (12)$$

where b^{-1} is of the scale of the horizon size, d_H , at the end of the QCDPT ($t \simeq 10^{-4}$ s), $b^{-1} = d_H \simeq \text{few km}$, while $M_n^{-1} \simeq 0.2fm$.

4.2 CMBR Polarization Correlations From Magnetic Wall

From Einstein's General Theory of Relativity (see, e.g., Kolb-Turner, "The Early Universe") $T(t)$, the temperature of the universe at time t is

$$kT(t) \simeq \frac{1\text{MeV}}{\sqrt{t(\text{in s})}}. \quad (13)$$

Using $380,000 \text{ years} = 1.2 \times 10^{13}$, $1 \text{ MeV} = 10^6 \text{ eV}$,

$$kT(t = 380,000 \text{ years}) \simeq 0.25 \text{ eV}. \quad (14)$$

Since the binding energy of electrons in hydrogen atoms is about 10 eV, electrons bound to atoms and were no longer free to scatter EM waves from the early universe. Light from the early universe was released: The CMBR.

CMBR TEMPERATURE CORRELATIONS:

Aim two microwave telescopes separated by the angle θ into the sky

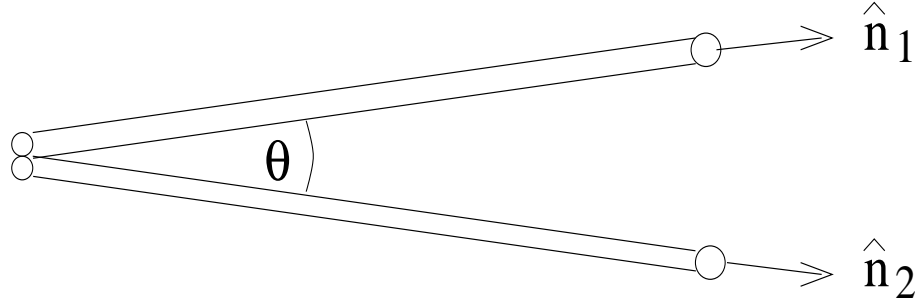


Figure 4:

Expand the temperature differences, $\Delta T(\hat{n}) = T(\hat{n}) - T_o$ in terms of angular functions

$$\begin{aligned} < \frac{\Delta T(\hat{n}_1)}{T_0} \frac{\Delta T(\hat{n}_2)}{T_0} > = \sum_{lm} C_l^{TT} Y_{lm}(\hat{n}_1) Y_{lm}(\hat{n}_2) \\ \text{use } \sum_m Y_{lm}(\hat{n}_1) Y_{lm}(\hat{n}_2) &= \frac{2l+1}{4\pi} P_l(\cos\theta) \\ \text{giving } < \frac{\Delta T(\hat{n}_1)}{T_0} \frac{\Delta T(\hat{n}_2)}{T_0} > &= \sum_l \frac{2l+1}{4\pi} C_l^{TT} P_l(\cos\theta) \end{aligned} \quad (15)$$

The P_l are well-known Legendre polynomials. The C_l^{TT} are the measured Temperature-Temperature correlations. From astrophysics observations COBE[7] WMAP[8] ACBAR[9] QUaD[10] the following was found:

- The universe is flat (space is not curved)
- Baryon density = 0.04 (4 % of density of universe)
- Dark Matter density = 0.23 (what is dark matter?)
- Dark energy density = 0.73 (vacuum energy)

CMBR B-B CORRELATIONS:

B-type polarization correlations, C_l^{BB} are derived from $\langle B_z(\mathbf{k}, \eta) B_z(\mathbf{k}', \eta) \rangle$, with $\mathbf{k} = k\hat{n}$ and η is conformal time, similar to C_l^{TT} being derived from $\langle \Delta T(\hat{n}_1) \Delta T(\hat{n}_2) \rangle$ (Eq(15)).

To get the power spectrum one must evaluate $\langle B_z(\mathbf{k}, \eta) B_z(\mathbf{k}', \eta) \rangle$. Using the fact that $\exp(-k^2 d_H^2) \simeq 1.0$ at the time of the QCDPT,

$$\begin{aligned} \langle B_z(\mathbf{k}, \eta) B_z(\mathbf{k}', \eta) \rangle &\simeq \mathcal{B}_W^2 \delta(k_x - k'_x) \delta(k_y - k'_y) \langle e^{-k_z^2/4M_n^2} e^{-k'^2/4M_n^2} \rangle \\ &\simeq \mathcal{B}_W^2 d_H e^{-k^2/4M_n^2} \delta(\mathbf{k} - \mathbf{k}'). \end{aligned} \quad (16)$$

This gives for the polarization power spectrum (see [6])

$$C_l^{BB} = \frac{(l+1)(l+2)}{\pi} \mathcal{B}_W^2 d_H \int dk \frac{j_l^2[k(\Delta\eta)]}{(\Delta\eta)^2}, \quad (17)$$

where the conformal time integral has been carried out and $\Delta\eta$ is the conformal time width at the last scattering. The integral over the spherical Bessel function is carried out by using the fact that $\int dz j_l^2(z) = \pi/(4l)$ for large l . Therefore in the range $100 < l < 2000$ one has the approximate result

$$C_l^{BB} \simeq \frac{25 d_H^5 B_W^2}{1152 M_n^2 \Delta\eta^3} l^2. \quad (18)$$

Using the parameters $M_n \Delta\eta = 1.5 \times 10^{39}$ [11], $d_H = 0.37 \times 10^{24} \text{ GeV}^{-1}$, and $B_W = 1.0 \times 10^{17}$ Gauss,

$$C_l^{BB} \simeq 4.25 \times 10^{-8} l^2 \quad (19)$$

The result for the B-type power spectrum is shown in Fig. 9 by the solid line.

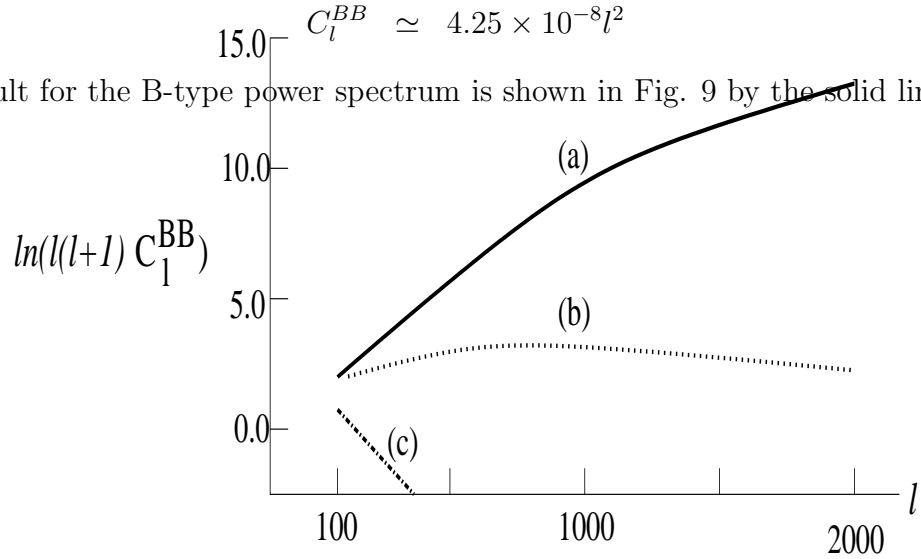


Figure 5: B power spectrum in (a) magnetic wall theory, (b) string theory, (c) inflation theory

The magnetic wall prediction for C_l^{BB} differs from other cosmological predictions, which should be measurable with the next generation of CMBR measurements.

5 Mixed Hybrid Heavy Quark Meson States

The Charmonium $\psi'(2S)$ and Upsilon $\Upsilon(3S)$ states, which are important for this review, are not consistent with being standard $c\bar{c}$ and $b\bar{b}$ mesons as has been shown by their decays into hadrons.

5.1 Heavy quark meson decay puzzles

A puzzle for Charmonium meson states is the ratio of branching ratios for $\psi'(2S)$ vs $J/\Psi(1S)$ to decay to hadrons. For example the $\rho - \pi$ puzzle: The $\Psi'(2S)$ to J/Ψ ratios for $\rho - \pi$ and decays are more than an order of magnitude smaller than predicted by the standard model[12, 13].

A puzzle for upsilin meson states is the two π decay, with the σ a broad 600 MeV $\pi - \pi$ resonance is:

$$\Upsilon(2S) \rightarrow \Upsilon(1S) + 2\pi \text{ large branching ratio. No } \sigma$$

$$\Upsilon(3S) \rightarrow \Upsilon(1S) + 2\pi \text{ large branching ratio to } \sigma$$

This has been called Vogel $\Delta n = 2$ Rule[14, 15]. Neither of these puzzles can be solved using standard QCD models. They were solved using the mixed heavy hybrid theory.

5.2 Mixed charmonium-Hybrid charmonium States

The method of QCD Sum Rules[16] was used to study the heavy quark Charmonium and Upsilon states, and show that two of them are mixed hybrid meson states[14]

The starting point of the method of QCD sum rules[16] for finding the mass of a state A is the correlator,

$$\Pi^A(x) = \langle |T[J_A(x)J_A(0)]| \rangle, \quad (20)$$

with $| \rangle$ the vacuum state and the current $J_A(x)$ creating the states with quantum numbers A. The following mixed vector ($J^{PC} = 1^{--}$) charmonium, hybrid charmonium current was used in QCD Sum Rules[14]

$$J^\mu = bJ_H^\mu + \sqrt{1-b^2}J_{HH}^\mu \quad (21)$$

with

$$\begin{aligned} J_H^\mu &= \bar{q}_c^a \gamma^\mu q_c^a \\ J_{HH}^\mu &= \bar{\Psi} \Gamma_\nu G^{\mu\nu} \Psi, \end{aligned} \quad (22)$$

where Ψ is the heavy quark field, $\Gamma_\nu = C\gamma_\nu$, γ_ν is the usual Dirac matrix, C is the charge conjugation operator, and the gluon color field is

$$G^{\mu\nu} = \sum_{a=1}^8 \frac{\lambda_a}{2} G_a^{\mu\nu}, \quad (23)$$

with λ_a the SU(3) generator ($Tr[\lambda_a \lambda_b] = 2\delta_{ab}$), discussed above.

Using QCD sumrules it was found[14] that the $\Psi'(2S)$ state is 50% normal and 50% hybrid. The analysis for upsilon states was similar, with the $\Upsilon(3S)$ being 50% normal and 50% hybrid:

$$|\Psi'(2s) \rangle = -0.7|c\bar{c}(2S) \rangle + \sqrt{1-0.5}|c\bar{c}g(2S) \rangle \quad (24)$$

$$|\Upsilon(3S) \rangle = -0.7|b\bar{b}(3S) \rangle + \sqrt{1-0.5}|b\bar{b}g(3S) \rangle \quad (25)$$

The QCD sum rule method is nonperturbative, has proved to be accurate in many calculations, with a 10% error in b , Eq(21), and M_B^2 .

6 Heavy Quark State Production In p-p and A-A Collisions

In order to discuss the possible detection of a QGP using the production of mixed heavy quark hybrids in A-A collisions (RHIC), we first review the earlier research on production of mixed heavy quark hybrids in p-p collisions, and then recent research on A-A collisions for $E=\sqrt{s}=200$ GeV.

6.1 Production of Ψ and Υ States In p-p Collisions

In this subsection we review the publication of [17] on heavy quark state production in unpolarized p-p collisions.

The color octet model[18, 19, 20, 21] was used. The three octet matrix elements needed are $\langle O_8^\Phi(^1S_0) \rangle$, $\langle O_8^\Phi(^3S_1) \rangle$, and $\langle O_8^\Phi(^3P_0) \rangle$, with Φ either J/Ψ , $\Psi'(2S)$, or $\Upsilon(nS)$. In [17] the second scenario of Nyayak and Smith[22] was used:

$$\langle O_8^\Phi(^1S_0) \rangle = .039 \quad \langle O_8^\Phi(^3S_1) \rangle = .0112 \quad \text{and} \quad \langle O_8^\Phi(^3P_0) \rangle = 0. \quad (26)$$

The differential production cross sections for Φ for helicity $\lambda = 0$ and 1 need the parameter A_Φ with

$$A_\Phi = \frac{5\pi^3\alpha_s^2}{288m^3s} \langle O_8^\Phi(^1S_0) \rangle, \quad (27)$$

with $s = E^2$, the strong coupling constant $\alpha_s \simeq 0.119$, and $m = 1.5$ or 5 GeV for the charmonium or bottomonium quark mass.

For the differential cross sections the rapidity variable, y , is used. The differential rapidity distributions for $\lambda = 0$, $\lambda = 1$ are given by (with $a = 4m^2/s$)

$$\frac{d\sigma_{pp \rightarrow \Phi(\lambda=0)}}{dy} = A_\Phi \frac{1}{x(y)} f_g(x(y), 2m) f_g(a/x(y), 2m) \frac{dx}{dy}, \quad (28)$$

$$\begin{aligned} \frac{d\sigma_{pp \rightarrow \Phi(\lambda=1)}}{dy} = & A_\Phi \frac{1}{x(y)} [f_g(x(y), 2m) f_g(a/x(y), 2m) + 0.613(f_d(x(y), 2m) f_{\bar{d}}(a/x(y), 2m) \\ & + f_u(x(y), 2m) f_{\bar{u}}(a/x(y), 2m))] \frac{dx}{dy}, \end{aligned} \quad (29)$$

with $f_g(x, 2m)$, $f_q(x, 2m)$ the gluonic and quark distribution functions evaluated at $Q = 2m$. See [17] for derivation of the factor 0.613. The variable $x(y)$ is

$$x(y) = 0.5 \left[\frac{m}{\sqrt{s}} (\exp y - \exp(-y)) + \sqrt{\left(\frac{m}{\sqrt{s}} (\exp y - \exp(-y)) \right)^2 + 4a} \right]. \quad (30)$$

Using CTEQ6[23] for $Q = 2m_c = 3$ GeV and $\sqrt{s} \simeq 200$ GeV, and for $Q = 2m_b = 10$ GeV and $\sqrt{s} \simeq 38.8$ GeV $f_g(x, 2m)$ and $f_q(x, 2m)$ were obtained.

Note that A_Φ is enhanced by a factor $\simeq \pi$ for the mixed hybrid $|\Psi'(2s)\rangle$ and $|\Upsilon(3S)\rangle$ states as derived in [17].

6.2 Charmonium Production Via Unpolarized p-p Collisions at $E=\sqrt{s}= 200$ Gev

For unpolarized p-p collisions with $\sqrt{s} = 200 \text{ GeV}$ using scenario 2[22], with the nonperturbative matrix elements given above, $A_\Phi = \frac{5\pi^3\alpha_s^2}{288m^3s} < O_8^\Phi(^1S_0) > = 7.9 \times 10^{-4} \text{ nb}$ for $\Phi = J/\Psi$; $a = 4m^2/s = 2.25 \times 10^{-4}$ for Charmonium. For $\sqrt{s} = 200 \text{ GeV}$ $x(y)$ is obtained from Eq(30) and

$$\frac{dx(y)}{dy} = \frac{M}{400} (\exp y + \exp(-y)) \left[1 + \frac{\frac{M}{200} (\exp y + \exp(-y))}{\sqrt{\left(\frac{M}{200} (\exp y - \exp(-y)) \right)^2 + 4a}} \right]. \quad (31)$$

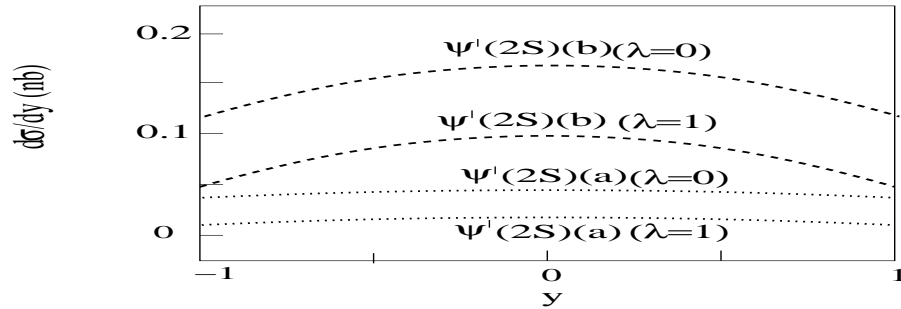


Figure 6: $d\sigma/dy$ for $Q= 3$ GeV, $E=200$ GeV unpolarized p-p collisions producing $\Psi'(2S)$ with $\lambda = 1, \lambda = 0$. Results labeled $\Psi'(2S)(a)$ are obtained using the standard model; results labeled $\Psi'(2S)(b)$ are obtained by using the mixed hybrid theory

Using Eqs(28,29,31), with the parton distribution functions given in Ref[17], we find $d\sigma/dy$ for $Q=3$ GeV, $\lambda = 0$ and $\lambda = 1$ the results for $\Psi'(2S)$ shown in Figure 6. The results for $d\sigma/dy$ shown in Figure 6 labeled $\Psi'(2S)(a)$ are obtained by using for the standard nonperturbative matrix element=0.039 times the matrix elements for J/Ψ production[17], while the results labeled $\Psi'(2S)(b)$ are obtained by using the mixed hybrid matrix element enhanced by a factor of π .

6.3 Upsilon Production Via Unpolarized p-p Collisions at $E=\sqrt{s}=38.8$ GeV

For $Q=10$ GeV, using the parton distributions given in Ref[17] and Eqs(28,29) for helicity $\lambda = 0$, $\lambda = 1$, with $A_\Upsilon = 5.66 \times 10^{-4}$ nb and $a = 6.64 \times 10^{-2}$, one obtains $d\sigma/dy$ for $\Upsilon(nS)$ production, $d\sigma/dy$ for $\Upsilon(3S)$ are shown in Figure 7.

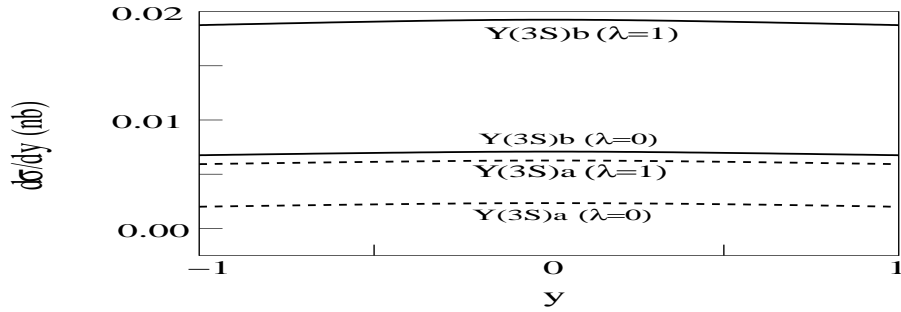


Figure 7: $d\sigma/dy$ for $Q=10$ GeV, $E=38.8$ GeV unpolarized p-p collisions producing $\Upsilon(3S)$ with $\lambda = 0$, $\lambda = 1$. The results for the standard model are labelled $\Upsilon(3S)a$, while for the hybrid theory are labelled $\Upsilon(3S)b$

In Fig. 7 as with $\Psi'(2S)$, the enhancement for $\Upsilon(3S)$ is a factor of π for the mixed hybrid theory vs. the standard model.

It should be noted that the ratios of $d\sigma/dy$ for $\Psi'(2S)$, and $\Upsilon(3S)$, for the hybrid theory vs. the standard are our most significant results. As will be discussed below, this might be used for detection of the QGP via relativistic energy A-A collisions (RHIC).

6.4 Heavy-quark state production in A-A collisions at $\sqrt{s_{pp}}=200$ GeV

This subsection is a review of [24], which is an extension of the theory of [17] for p-p to A-A collisions.

The differential rapidity cross section for the production of a heavy quark state with helicity $\lambda = 0$ in the color octet model in A-A collisions is given by

$$\frac{d\sigma_{AA \rightarrow \Phi(\lambda=0)}}{dy} = R_{AA}^E N_{bin}^{AA} < \frac{d\sigma_{pp \rightarrow \Phi(\lambda=0)}}{dy} >, \quad (32)$$

where R_{AA}^E is the product of the nuclear modification factor R_{AA} and S_Φ , the dissociation factor after the state Φ (a charmonium or bottomonium state) is formed (see [25]). N_{bin}^{AA} is the number of binary collisions in the AA collision, and $< \frac{d\sigma_{pp \rightarrow \Phi(\lambda=0)}}{dy} >$ is the differential rapidity cross section for Φ production via nucleon-nucleon collisions in the nuclear medium. Note that R_{AA}^E , which we take as a constant, can be functions of rapidity [26, 27].

Experimental studies show that for $\sqrt{s_{pp}} = 200$ GeV $R_{AA}^E \simeq 0.5$ both for Cu-Cu [25, 28] and Au-Au [29, 30, 31]. The number of binary collisions are $N_{bin}^{AA} = 51.5$ for Cu-Cu [32] and 258 for Au-Au. The differential rapidity cross section for pp collisions in terms of f_g , the gluon distribution function ($-0.8 \leq y \leq 0.8$ for $\sqrt{s_{pp}} = 200$ GeV with f_g from [17]), is

$$< \frac{d\sigma_{pp \rightarrow \Phi(\lambda=0)}}{dy} > = A_\Phi \frac{1}{x(y)} f_g(\bar{x}(y), 2m) f_g(a/\bar{x}(y), 2m) \frac{dx}{dy}, \quad (33)$$

where $a = 4m^2/s$; with $m = 1.5$ GeV for charmonium, and 5 GeV for bottomonium. For $\sqrt{s_{pp}} = 200$ GeV $A_\Phi = 7.9 \times 10^{-4}$ nb for $\Phi = J/\Psi$ and 2.13×10^{-5} nb for $\Upsilon(1S)$; $a = 2.25 \times 10^{-4}$ for Charmonium and 2.5×10^{-3} for Bottomium.

The function \bar{x} , the effective parton x in a nucleus (A), is given in [33, 34]:

$$\begin{aligned} \bar{x}(y) &= x(y) \left(1 + \frac{\xi_g^2 (A^{1/3} - 1)}{Q^2} \right) \\ x(y) &= 0.5 \left[\frac{m}{\sqrt{s_{pp}}} (\exp y - \exp(-y)) + \sqrt{\left(\frac{m}{\sqrt{s_{pp}}} (\exp y - \exp(-y)) \right)^2 + 4a} \right], \end{aligned} \quad (34)$$

with [35] $\xi_g^2 = .12 GeV^2$. For J/Ψ $Q^2 = 10 GeV^2$, so $\bar{x} = 1.058x$ for Au and $\bar{x} = 1.036x$ for Cu, while for $\Upsilon(1S)$ $Q^2 = 100 GeV^2$, so $\bar{x} = 1.006x$ for Au and $\bar{x} = 1.004x$ for Cu.

From Eqs(32,33,34) and the parameters given above one finds the differential rapidity cross sections for J/Ψ , $\Psi(2S)$, and $\Upsilon(nS)$ states for A-A collisions.

The differential rapidity cross sections for $\Psi(2S)$ and $\Upsilon(3S)$ production via Cu-Cu and Au-Au collisions at RHIC (E=200 GeV) are shown in the figures below for both the standard model and the mixed hybrid theory with the cross sections enhanced by π with the mixed hybrid theory, as discussed above.

The absolute magnitudes are uncertain, and the shapes and relative magnitudes are the main prediction.

The differential rapidity cross sections are shown in the following figures for $\Psi(2S)$ and $\Upsilon(3S)$ mixed hybrid state production via Cu-Cu, Au-Au collisions ($E=200$ GeV).

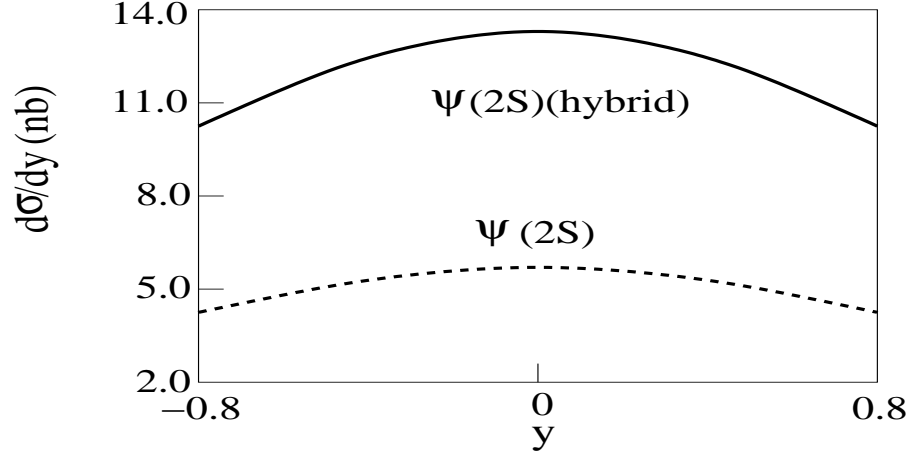


Figure 8: $d\sigma/dy$ for $2m=3$ GeV, $E=200$ GeV Cu-Cu collisions producing $\Psi(2S)$ with $\lambda = 0$. The dashed curve is for the standard $c\bar{c}$ model.

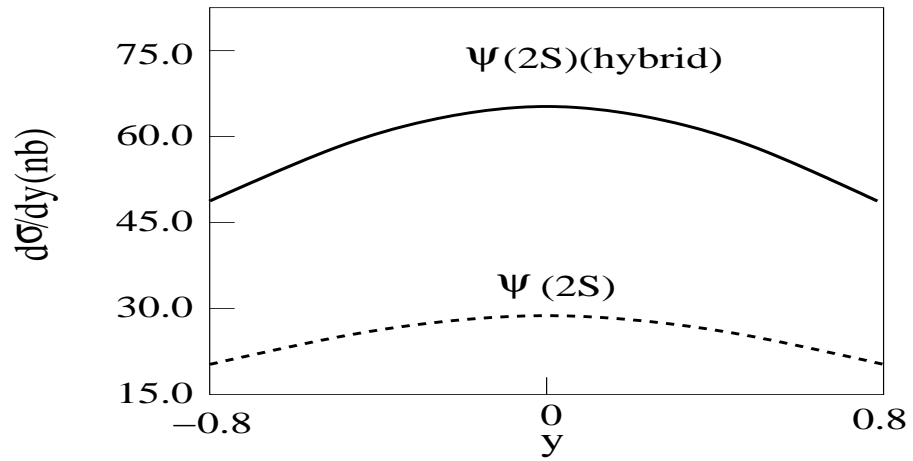


Figure 9: $d\sigma/dy$ for $2m=3$ GeV, $E=200$ GeV Au-Au collisions producing $\Psi(2S)$ with $\lambda = 0$. The dashed curve is for the standard $c\bar{c}$ model.

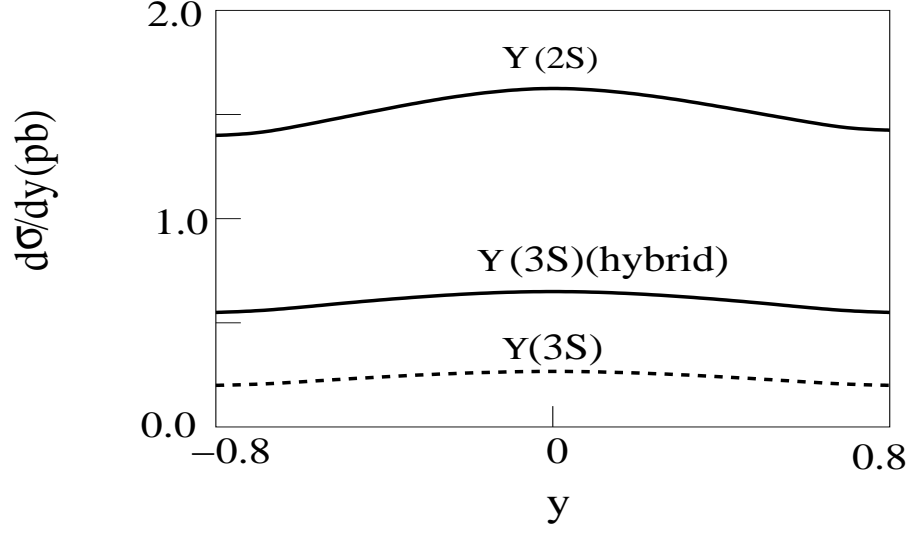


Figure 10: $d\sigma/dy$ for $2m=10$ GeV, $E=200$ GeV Cu-Cu collisions producing $\Upsilon(2S)$, $\Upsilon(3S)$ with $\lambda = 0$. For $\Upsilon(3S)$ the dashed curve is for the standard $b\bar{b}$ model.

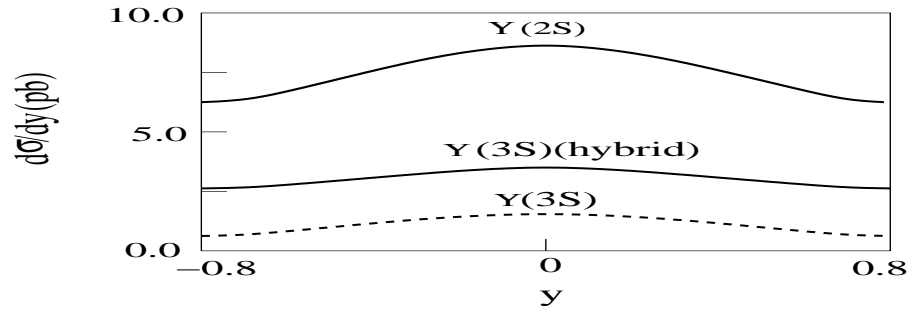


Figure 11: $d\sigma/dy$ for $2m=10$ GeV, $E=200$ GeV Au-Au collisions producing $\Upsilon(2S)$, $\Upsilon(3S)$ with $\lambda = 0$. For $\Upsilon(3S)$ the dashed curve is for the standard $b\bar{b}$ model.

6.5 Creation of the QGP

At Brookhaven National Lab (BNL) the energy has been increased so that with RHIC, such as Pb-Pb collisions, the energy of the atomic nuclei is large enough so just after the nuclei collide the temperature is that of the universe about 10^{-5} seconds after the Big Bang. That is $kT_c^{QCDPT} \simeq 150$ MeV. This results in the reverse QCDPT during which the nucleons, consisting of three quarks bound by interactions with gluons, transform to the QGP, a dense plasma of quarks and gluons. This is illustrated in the figure below.

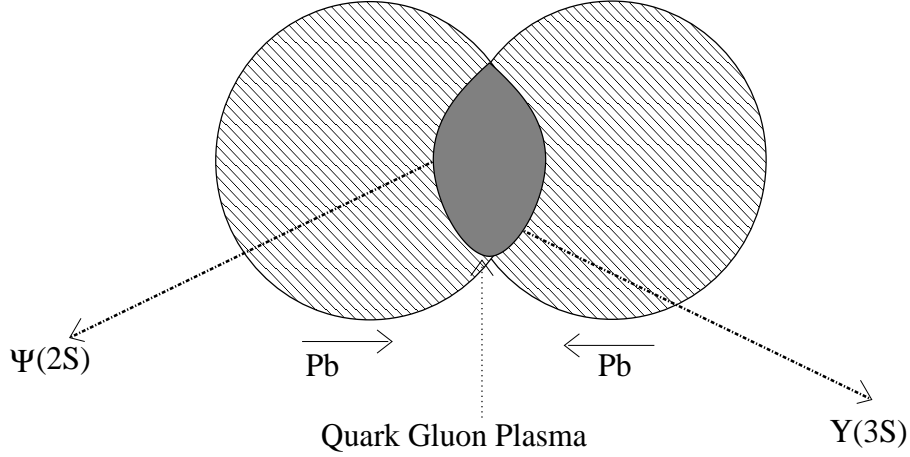


Figure 12: Pb-Pb collisions producing the QGP, which produces $\Psi(2S)$ and $\Upsilon(3S)$ states.

6.6 Detection of the QGP via Hybrid Heavy Quark State Production

Because of the active gluons in the hybrid components of $\Psi(2S)$ and $\Upsilon(3S)$ heavy quark mesons, the production of these mixed hybrid states by the QGP, which also has active gluons, is a possible test of the creation of the QGP via RHIC.

This would be a remarkable achievement for nuclear and particle physics. It would also be important for cosmology, in which it is believed that the universe before 10^{-5} seconds after the Big Bang consists of the QGP, but no experimental evidence of the QCD exists at the present time.

In summary, in future experiments at BNL and the LHC-CERN the study of RHIC producing $\Psi(2S)$ and $\Upsilon(3S)$ mixed hybrid mesons could be a method for determining the creation of the QGP via atomic nuclei colliding with an energy large enough to create matter with a temperature T_c^{QCDPT} , the critical temperature for the cosmological phase transition from the QGP to our present universe with nucleons.

6.7 Ratios of $\Psi'(2S)$ to J/Ψ and $\Upsilon(2S)$, $\Upsilon(3S)$ to $\Upsilon(1S)$ cross sections cross sections

Since the cross section ratios of the standard and mixed hybrid Ψ and Υ states were discussed in detail in Ref[1], we shall not review these ratios.

7 $\Psi(2S)$, $\Upsilon(3S)$ Suppression in p-Pb, Pb-Pb Collisions and Mixed Hybrid Theory

The suppressin of Ψ and Υ states in passing through a nucleus is discussed in Ref[36, 37, 38]

The probability for production of a heavy quark meson state Φ on a nucleus, with A the number of nucleons, irrelative to a nucleon, is the suppression S_A with

$$S_A = e^{-n_o \sigma_{\Phi N} L}, \quad (35)$$

where L is the length of the path of Φ in nuclear matter $\simeq 10$ fm for p-Pb collisions and 15 fm for Pb-Pb collisions, $\sigma_{\Phi N}$ is the cross section for Φ -nucleon collisions, and the nuclear matter density $n_o \simeq .07 fm^{-3}$. Note that in Refs[37, 38] there were typos sith $n_o = .017 fm^{-3}$.

7.1 $\Psi(2S)$ to $J/\Psi(1S)$ suppression in p-Pb collisions

The cross section for standard charmonium $c\bar{c}$ meson via strong QCD interactions with nucleons is given by[36]

$$\sigma_{c\bar{c}N} = 2.4\alpha_s \pi r_{c\bar{c}}^2, \quad (36)$$

where the strong coupling constant $\alpha_s \simeq 0.118$, and the charmonium meson radius $r_{c\bar{c}} \simeq h/(2M_c c)$, with M_c the charm quark mass. Using $2M_c \simeq M_{J/\Psi} \simeq 3$ GeV, $r_{c\bar{c}} \simeq \hbar/(3GeV c) \simeq 6 \times 10^{-17} m = 0.06 fm$, giving

$$\sigma_{c\bar{c}N} \simeq 3.2 \times 10^{-3} fm^2 = 3.2 \times 10^{-2} mb. \quad (37)$$

Therefore $n_o \sigma_{c\bar{c}N} L \simeq 0.0022$ and

$$S_A^{c\bar{c}} = e^{-n_o \sigma_{c\bar{c}N} L} \simeq 1.0. \quad (38)$$

The cross section for hybrid charmonium $c\bar{c}g$ meson via strong QCD interactions with nucleons has been estimated in Ref[36] as $\sigma_{c\bar{c}gN} \simeq 6.5$ mb. Therefore, $n_o \sigma_{c\bar{c}gN} L \simeq 1.1$, and

$$S_A^{c\bar{c}g} \simeq 0.33. \quad (39)$$

Using the mixed hybrid theory for $\Psi(2S)$, with 50% $|c\bar{c}\rangle$ and 50% $|c\bar{c}g\rangle$, the relative suppression of $\Psi(2S)$ to $J/\Psi(1S)$ is

$$\begin{aligned} R^{\Psi(2S)-J/\Psi(1S)}|_{theory} &\simeq \frac{1+0.33}{2} \\ &= 0.66. \end{aligned} \quad (40)$$

The experimental result[?] is

$$R^{\Psi(2S)-J/\Psi(1S)}|_{exp} \simeq 0.65 \pm 0.1, \quad (41)$$

therefore the theory agrees with the experiment within errors.

7.2 Suppression of $\Upsilon(3S)/\Upsilon(1S)$ in Pb-Pb Collisions

The experimental results for the ratio of ratios needed for the present subsection is[39] is

$$\frac{\Upsilon(3S)/\Upsilon(1S)|_{PbPb}}{\Upsilon(3S)/\Upsilon(1S)|_{pp}} = 0.06 \pm 0.06(\text{stat}) \pm 0.06(\text{syst}); . \quad (42)$$

Using $\sigma_{b\bar{b}N} \simeq \sigma_{c\bar{c}N}(M_c/M_b)^2 \simeq 0.09\sigma_{c\bar{c}N}$, one obtains for the $b\bar{b}$ component of $\Upsilon(3S)$

$$S_A^{b\bar{b}} = \frac{\Upsilon(3S)/\Upsilon(1S)|_{PbPb}}{\Upsilon(3S)/\Upsilon(1S)|_{pp}}|_{sm} \simeq 0.11 . \quad (43)$$

For the hybrid bottomonium $b\bar{b}g$ meson $\sigma_{b\bar{b}gN} = \sigma_{c\bar{c}gN}(M_c/M_b)^2 \simeq 0.09\sigma_{c\bar{c}gN} \simeq 0.059 fm^2$, and with $L \simeq 15$ fm for Pb-Pb collisions, $n_o\sigma_{b\bar{b}gN}L \simeq 0.15$, giving $S_A^{b\bar{b}g} \simeq 0.017$. From this and Eq(43) one finds[37]

$$\begin{aligned} R^{\Upsilon(3S)-\Upsilon(1S)}|_{theory} &\simeq \frac{.11 + .017}{2} \\ &\simeq 0.06 , \end{aligned} \quad (44)$$

in agreement with the experimental ratio shown in Eq(42), within experimental and theoretical errors.

Similar results for $\Psi(2S)$ and $\Upsilon(3S)$ supression in p-Pb collisions at an energy of 8 TeV can be found in Ref[38]

8 Conclusions

The creation of a magnetic wall during the QCDPT, with B-B CMBR correlations is reviewed. This is a prediction for future cosmological CMBR studies, and a test of the theory of the cosmological QCDPT.

Then the use of QCD sum rules to show that the $\Psi(2S)$ and $\Upsilon(3S)$ are approximately 50% normal $|q\bar{q} >$ states and 50% hybrid $|q\bar{q}g >$ states was briefly reviewed.

The differential rapidity cross sections for J/Ψ , $\Psi(2S)$ and $\Upsilon(nS)(n = 1, 2, 3)$ production via p-p collisions was reviewed. The enhancement of the production of $\Psi(2S)$ and $\Upsilon(3S)$ mixed heavy quark states was shown to be in agreement with experiments. This is an important result for the test of the production of QGP via RHIC.

The differential rapidity cross sections for Ψ and Υ production via Cu-Cu and Au-Au collisions at RHIC (E=200 GeV) using R_{AA}^E , the product of the nuclear modification factor R_{AA} and the dissociation factor S_Φ , N_{bin}^{AA} the binary collision number, and the gluon distribution function should give some guidance for future RHIC experiments. Then the possibly detection of the QGP via RHIC at the BNL and LHC was reviewed.

Finally, recent research on the suppression of heavy quark states, especially hybrid heavy quark states, produced via RHIC, as these mesons travel through nuclear matter was reviewed.

Acknowledgements

The author acknowledges many helpful discussions with Dr. Debasish Das, Saha Institute of Nuclear Physics, India, and support from the P25 group at Los Alamos National Laboratory.no

References

- [1] Leonard S. Kisslinger, Debasish Das, Int. J. Mod. Phys. **31**, 163001 (2016)
- [2] Ta-Pei Cheng and Ling-Fong Li, “Gauge theory of elementary particle physics”, Oxford University Press (1984)
- [3] Zhou Li-juan, Ma Wei-xing, Leonard S. Kisslinger, J. Mod. Phys. **3**, 1172 (2012)
- [4] Leonard S. Kisslinger, Phys. Rev. **D 68**, 043516 (2003)
- [5] M.M. Forbes and A.R. Zhitnitsky, Phys. Rev. Lett. **85**, 5268 (2000)
- [6] Wayne Hu and Martin White, Phys. Rev. **D 56**, 596 (1997)
- [7] D.J. Fixsen et. al., COBE (COspheric Background Explorer), Astrophys. J. **473**, 576 (1996)
- [8] G. Hinshaw et. al., WMAP (Wilkinson Microwave Anisotropic Probe), arXiv:[astro-ph]1212.5226 (2013)
- [9] C.L. Reichart et. al., ACBAR (Arcminute Cosmology Bolometer Array Receiver), Astrophys. J. **674**, 1200 (2008)
- [10] S. Gupta et. al., QUaD (QUEST and DASI), Astrophys. J. **716**, 1040 (2010)
- [11] T.R. Seshadri and K.Subramanian, Phys. Rev. Lett. **87**, 101301 (2001).
- [12] M.E.B. Fraklin et. al. (Mark II Collaboration) Phys. Rev. Lett. **51**, 963 (1983)
- [13] L.S. Kisslinger, D. Parno, S. Riordan, Adv. High Energy Phys. 2009:9822341 (2009)
- [14] L.S. Kisslinger, Phys. Rev. **D 79**, 114026 (2009)
- [15] H. Vogel, Proceedings of 4th Flavor Physics and CP Violation Conference (FPCP’06) (2006)
- [16] M.A. Shifman, A.I. Vainstein and V.I. Zakharov, Nucl. Phys. **B147**, 385 (1979); Nucl. Phys. **B147** 448 (1979)
- [17] Leonard S. Kisslinger, Ming X. Liu and Patrick McGaughey, Phys. Rev. **D 84**, 114020 (2011)
- [18] P.L Cho and A.K. Leibovich, Phys. Rev. **D 53**, 150 (1996)

- [19] E. Braaten and Y-Q Chen, Phys. Rev. **D 54**, 3216 (1996)
- [20] E. Braaten and S. Fleming, Phys. Rev. Lett. **74**, 3327 (1995)
- [21] P.L Cho and A.K. Leibovich, Phys. Rev. **D 53**, 6203 (1996)
- [22] G.C. Nayak and J. Smith, Phys. Rev. **D 73**, 014007 (2006)
- [23] CTEQ6: hep.pa.msu.edu/cteq/public/cteq6.html
- [24] Leonard S. Kisslinger, Ming X. Liu and Patrick McGaughey, Phys. Rev. **C 89**, 024914 (2014)
- [25] B.I. Abelev *et al* (STAR Collaboration), Phys. Rev. **C 80**, 041902 (2009)
- [26] A.D. Frawley, T. Ullrich, and R. Vogt, Phys Rep. **462**, 125 (2008)
- [27] Rishi Sharma and Ivan Vitev, Phys. Rev. **C 80**, 044905 (2013)
- [28] A. Adare *et al* (PHENIX Collaboration) Phys. Rev. Lett. **101**, 122301 (2008)
- [29] A. Adare *et al* (PHENIX Collaboration) Phys. Rev. Lett **98**, 172301 (2007)
- [30] B.I. Abelev *et al* (STAR Collaboration) Phys. Rev. Lett. **98**, 192301 (2007)
- [31] F. Karsch, D. Kharzeev and H. Satz, Phys. Lett. **B 637**, 75 (2006)
- [32] S. Baumgart (STAR), arXiv:0709.4223/nuc-ex
- [33] I. Vitev, T. Goldman, M.B. Johnson, and J.W. Qiu, Phys. Rev. **D 74**, 054010 (2006)
- [34] R. Sharma, I. Vitev, and B-W. Zhang, Phys. Rev. **D 80**, 054902 (2009)
- [35] J.W. Qiu and I. Vitev, Phys. Rev. Lett. **93**, 262301 (2004)
- [36] D. Kharzeev and H. Satz, arXiv:9508276[hep-ph] (1995)
- [37] Leonard S. Kisslinger, Int. J. Theor. Phys. **54**, 1847 (2016)
- [38] Leonard S. Kisslinger and Debasish Das, Int. J. Theor. Phys. **55**, 1847
- [39] S.Chatrchyan *et al*, CMS Collaboration, Phys. Rev. Lett. **109**, 222301 (2012)